DLP 3D – printing of shape memory polymers stabilized by thermoreversible hydrogen bonding interactions

DLP 3D – printing of shape memory polymers stabilized by thermoreversible hydrogen bonding interactions

*Andrea Cosola, Marco Sangermano, Davide Terenziani, Riccardo Conti, Massimo Messori, Hansjörg Grützmacher and Annalisa Chiappone**

A. Cosola, Prof. M. Sangermano and Dr. A. Chiappone
Department of Applied Science and Technology
Politecnico di Torino
Torino 10129, Italy
E-mail: annalisa.chiappone@polito.it

D. Terenziani and Prof. M. Messori,
Department of Engineering "Enzo Ferrari"
University of Modena and Reggio Emilia
Modena 41125, Italy

R. Conti and Prof. H. Grützmacher
Department of Chemistry and Applied Biosciences
Laboratory of Inorganic Chemistry
ETH Zürich
Zürich 8093, Switzerland

Keywords: 3D Printing; DLP; shape memory polymers; smart materials; multifunctional photoinititator.

Abstract: In this paper a photopolymerizable system based on 2-hydroxyethyl methacrylate (HEMA) and poly(ethylene glycol methyl ether methacrylate) (PEGMEMA) is used for the fabrication of shape memory polymers (SMPs) *via* digital light processing (DLP) three-dimensional (3D)-printing. A bis(acyl)phosphane oxide derivative (BAPO-γ-CyD) was used as an all-in-one photoinitiator and crosslinking agent. Due to the high elasticity ratio between the glassy and rubbery state and the presence of thermoreversibly associating hydrogen-bonding groups, the PHEMA-*co*-PEGMEMA polymers show an excellent thermally triggered shape memory response (strain recovery of 99%). A prototype of a thermoresponsive airflow diverter has been fabricated, demonstrating the potential integration of such SMPs to develop smart 3D – printed devices. Moreover, the possibility to easily design the glass transition temperature of the SMPs by varying the concentration of the two photopolymerizable ingredients allows to

fine-tune the formulations such that materials can be printed showing shape memory behavior at different temperatures.

1. Introduction

In the last years, stimuli-responsive polymers have gained increasing interest due to their widespread use ranging from biomedical,[1–3] aerospace[4,5] and automotive applications,[6] to microfluidics[7,8] and microelectronics.[9,10] Belonging to this class of smart materials, shape memory polymers (SMPs) are capable of recovering their original shape from a temporary deformed configuration upon exposure to an external trigger, such as heat, electricity, magnetism, light and pH variation.[11–13]

Temperature is currently the most widely investigated triggering mechanism. To get a thermally-activated shape memory response, a polymer requires a specific molecular architecture consisting of chemical or physical netpoints to set the permanent shape, and a reversible switching phase controlled by a transition temperature (T_{trans}), such as the melting temperature (T_m) or the glass transition temperature (T_g), to program a temporary shape.[14–17] In a traditional thermally-activated shape memory cycle, a SMP is heated above the transition temperature of its switching phase ($T > T_{trans}$) to reach a rubbery state. At this point the material is simply deformed by the application of mechanical stress. The temporary shape is then fixed by cooling the strained polymer below the transition temperature ($T < T_{trans}$). The thermodynamically more stable permanent shape can be recovered *via* an entropy-driven process upon heating the material above T_{trans}.

The typical strategy for the preparation of thermoresponsive SMPs relies on using semi-crystalline polymers [e.g. poly(caprolactone), PCL] as molecular switching phase. Accordingly, the temporary shape is stabilized below T_m (more precisely, below crystallization temperature, T_c) by the generation of crystalline domains, while recovery of the shape is reached by heating

again to above T_m where the crystalline phase is destroyed and the chain mobility is regained.[18–21]

Apart from this rather conventional approach, the use of amorphous polymers containing reversible binding groups (RBGs), either non-covalent or covalent, has emerged as an alternative strategy for the preparation of SMPs.[14] Among all the non-covalent RBGs, hydrogen bonding motifs are of particular interest due to their thermoreversibility, that is within a dynamic hydrogen bonding network, hydrogen bonds between a donor and acceptor group constantly break and reform depending on the temperature. The re-association of hydrogen bonds at $T < T_{trans}$ allows to generate temporary non-covalent networks that stabilize the programmed shape at low temperatures.[22–25]

More recently, the use of SMPs in additive manufacturing (AM) led to an exciting extension of 3D-printing, defined by Tibbit as four dimensional (4D) printing.[26] Indeed, the processing of materials capable of transforming with time under the application of an external trigger introduces an additional fourth dimension, giving the opportunity to overcome the static nature of the traditional 3D – printed structures.[27–31]

In this study, we investigate a solvent-free photopolymerizable system based on monofunctional methacrylates containing groups which thermoreversibly form H-bonds for the fabrication of 3D-printable SMPs by means of digital light processing (DLP). In such a system, 2-hydroxyethyl methacrylate (HEMA) and poly(ethylene glycol) methyl ether methacrylate (PEGMEMA) were used as photopolymerizable ingredients. No additional cross-linkers are included since the phosphaneoxide derivative (BAPO-γ-CyD) used as multifunctional photoinitiator (MFPI) serves simultaneously as photocrosslinking agent, as reported in a previous work.[32] Prior to 3D-Printing the photopolymerization kinetics of the system is investigated by means of real-time photorheology. Dynamic mechanical thermal analyses (DMTAs) were carried out to evaluate the influence of the formulation ingredients on the thermo-mechanical properties of the cured PHEMA-*co*-PEGMEMA polymers. The thermally

activated shape memory behavior was investigated both qualitatively, simply by evaluating the capability of different 3D-printed structures to recover their original shape from a deformed configuration, and quantitatively, with the analysis of the shape memory response of the photocured polymers under the application of properly designed thermo-mechanical cycles. At last, a prototype of thermoresponsive airflow diverter has been developed, as a proof of concept, to demonstrate the potential integration of such SMPs in the fabrication of smart devices.

2. Results and discussion

As already reported in a previous study, the γ-cyclodextrin bis(acyl)phosphaneoxide derivative (BAPO-γ-CyD) was successfully prepared from multi-acrylated γ-cyclodextrin and bis(2,4,6-trimethylbenzoyl)-hydrogenphosphane, following a convergent synthesis. This multifunctional photoinitiator (MFPI) stands out by serving as photocrosslinking agent for monofunctional methacrylate monomers, due to its multi-photoactive groups. Therefore, thermosetting networks can be generated simply exploiting the all-in-one properties of the photoinitiator, with no need of additional crosslinkers.[32] Looking at the photopolymerizable system chosen in this work, covalently crosslinked PHEMA-*co*-PEGMEMA branched networks can be generated by radical copolymerization of HEMA and PEGMEMA either *via* the PO-γCyD groups formed during the photolysis of BAPO-γ-CyD or via its residual acrylate functions (**Scheme 1**).

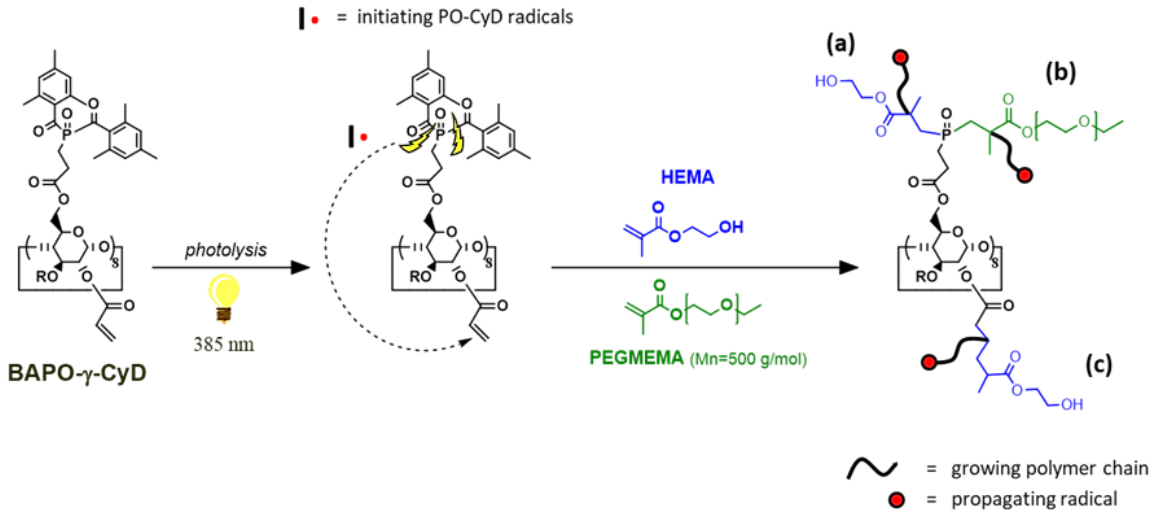

Scheme 1. Crosslinked covalent PHEMA-*co*-PEGMEMA network generated either *via* PO-CyD groups or residual acrylate functions of the multifunctional photoinitiator BAPO-γ-CyD. Three possible scenarios for polymerization and cross-linking are shown: a) top-left: polymerization of HEMA; b) top-right: polymerization of PEGMEMA; c) bottom: involvement of acrylate functions of BAPO-γ-CyD in polymer formation.

The photopolymerization of the photocurable system was investigated prior to 3D–printing by means of photorheology. Several formulations, denoted as HxPy, where x and y correspond to the weight concentration of HEMA and PEGMEMA, respectively, were prepared. Preliminary studies were carried out to evaluate the influence of different amount of BAPO-γ-CyD on the curing kinetics. For this purpose, the two monomers were used at constant weight ratio 1:1 (H50P50), while the concentration of the MFPI is varied between 0.1 and 2.0 parts per hundred resin (phr). Both the irradiation time required to induce crosslinking (induction time, t_{ind}) and the time to reach the crossover between the loss and the storage moduli (gel time, t_{gel}) were recorded.

The data reveal that both t_{ind} and t_{gel} decrease from 29 to 16 s and from 106 to 35 s, respectively, by increasing the concentration of the MFPI. However, since the values seems to reach a plateau when the MFPI is used above 1.5 phr (**Figure 1a** and **Figure 1b**), we decided to set the concentration of MFPI to this value. Then, three different formulations were prepared by varying the HEMA:PEGMEMA weight ratio (**Table 1**). Once again, the photopolymerization kinetics of the formulations were investigated. The results reveal that the polymerization rate increases from 0.6 to 6.2 MPa/s by increasing the concentration of HEMA in the precursor formulation, as suggested by the steeper slopes of the curves reported in **Figure 1c**. This is likely due to the much higher reactivity of HEMA with respect to PEGMEMA, as confirmed by the curing kinetics of pure HEMA or PEGMEMA.

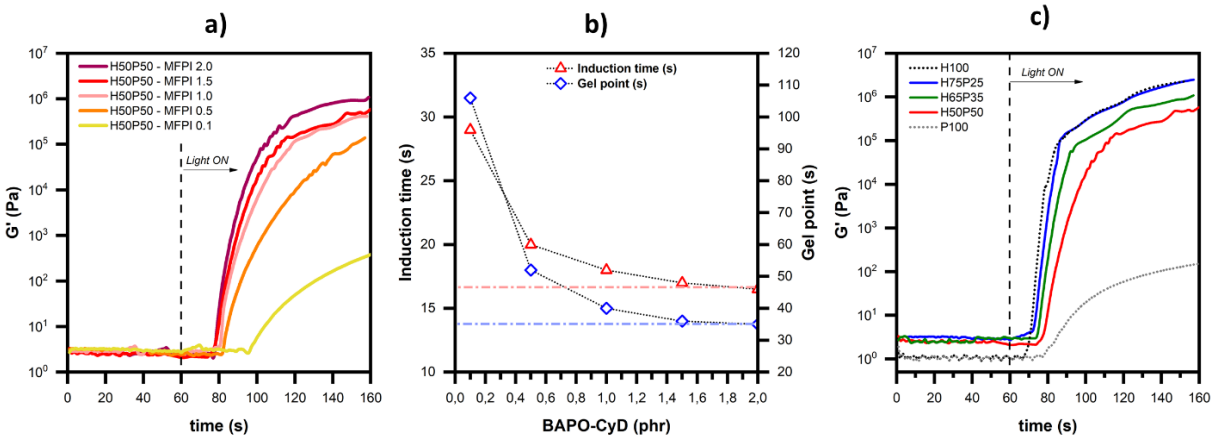

Figure 1. a) Photorheology curves corresponding to the photopolymerization kinetics of H50P50 (taken as reference formulation) at different concentration of BAPO-γ-CyD; b) influence of BAPO-γ-CyD on t_{ind} and t_{gel} and c) photorheology characterization of the final photocurable formulations prepared by varying the HEMA/PEGMEMA weight ratio (the dotted lines are referred to two standard formulations with either 100% HEMA or 100% PEGMEM and 1.5 phr of BAPO-γ-CyD used as reference). For all the experiments, the light was switched on after 60 s to let the system stabilize before the onset of photopolymerization.

Table 1. Composition and photorheological properties of the final precursor formulations tested for DLP 3D-Printing and further investigations.

Formulation code	Composition			Photorheology data		
	HEMA [wt%]	PEGMEMA [wt%]	BAPO-γ-CyD [phr]	t_{ind} [s]	t_{gel} [s]	ΔG/Δt [Mpa/s]
H50P50	50	50	1.5	16	34	0.8
H65P35	65	35	1.5	15	27	2.4
H75P25	75	25	1.5	13	22	6.4

This last set of formulations given in Table 1 was tested for DLP 3D-Printing [a dye is added (0.025 phr) to increase the printing resolution] and the photocured polymers obtained from these formulations were used for further investigations.

The printability of the chosen photocurable system was demonstrated by successfully printing various CAD models using an ASIGA UV-MAX X27 DLP printer (**Figure 2**). High values of gel content were obtained from all printed polymers (up to 94%, **Figure S1** in the Supporting Informations), confirming the efficiency of the multifunctional photoinitiator BAPO-γ-CyD as crosslinking agent and proving that no additional crosslinkers are needed for the printing process.

Figure 2. Photographs of several 3D-Printed structures from the final set of formulations (L=1 cm).

Dynamic mechanical thermal analyses (DMTAs) were carried out to evaluate the influence of the formulation ingredients on the mechanical properties of the photocured polymers (denoted as PHEMA-*co*-PEGMEMA X:Y, where X and Y refers to weight concentration of HEMA and PEGMEMA in the precursor formulation). The results revealed that the glass transition temperature (T_g) of the PHEMA-*co*-PEGMEMA polymers increases with the concentration of HEMA in the precursor formulation, as evidenced by the shift of the tanδ peak from 12°C to 63°C (**Figure 2a**). Moreover, a gradual but significant drop of the mechanical properties is observed in the E' plots between the glassy and rubbery plateau. By way of example, the drop of the properties is represented schematically in **Figure 2b**, which show the different behavior of a small rectangular specimen from PHEMA-*co*-PEGMEMA 75:25 in bearing a load of either 50 g or 2 g below and above its T_g.

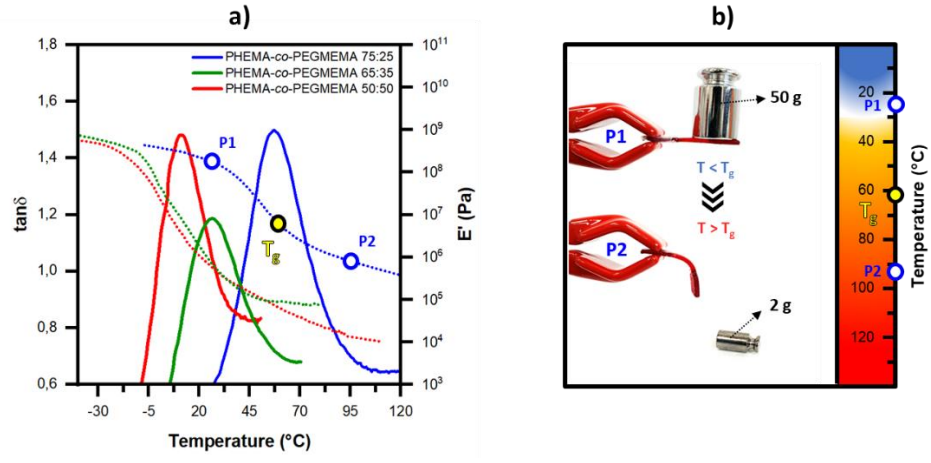

Figure 2. a) Conservative modulus (E') and damping factor (tanδ) plots, as determined by DMTAs for all the different precursor formulations being investigated; b) picture of a small rectangular specimen from PHEMA-*co*-PEGMEMA 75:25 bearing a load of 50 g below and 2 g above its T_g (P1 and P2, respectively).

As well-established in the literature,[33,34] hydrogen-bonding is an important factor in determining the glass transition temperature of a polymer, although it is not the only one.

In fact, it has been proven that the T_g increases linearly with the concentration of either strong or weak H-bonding groups, since the H-bonds restrict the motion of the polymer chains behaving as temporary physical crosslinks of a supramolecular network. Therefore, it is reasonable to suppose that the thermomechanical behavior of the investigated PHEMA-*co*-PEGMEMA polymers is affected by the generation of a non-covalent network.

Multiple H-bonding interactions can occur *via* the side terminal hydroxyl groups (OH) of PHEMA, which can act as both proton donor and proton acceptor, and the proton accepting carbonyl groups (C=O) of both PHEMA and PEGMEMA. Vibrational spectroscopy can be used to investigate H-bonding interactions.[35] Both the broad and overlapping bands of the hydroxyl groups (νOH: 3700 – 3000 cm^{-1}) and the stretching vibrations of the carbonyl groups (νC=O: 1730 – 1700 cm^{-1}) allow to evaluate the formation of a H-bonding network through the side terminal OH groups of PHEMA. The specific H-bonding vibrations in the aforementioned spectral regions are typically identified in the second derivative spectra and *via* fitting analyses and their assignment has been thoroughly investigated in the literature.[36–38]

Upon fitting the OH stretching bands, three Gaussian components can be easily identified which correspond to the νOH bands of H-bonded O-H···O=C and O-H···O-H aggregates at around 3530 and 3320 cm^{-1}, and to the first overtone of C=O stretching at 3430 cm^{-1}. The overlapping C=O stretching vibrations were deconvoluted into two absorptions, one at 1730 cm^{-1} and the other at 1703 cm^{-1}, that are assigned to free C=O and H-bonded C=O groups, respectively. The intermolecular H-bonding interactions in the PHEMA-*co*-PEGMEMA polymers are likewise confirmed by analyses of the IR spectra (**Figure 3a** and **Figure S2**). The characteristic absorptions corresponding to H-bonded O-H···O=C and O-H···O-H aggregates can be identified in both the second derivative spectra and the fitted spectra of all PHEMA-*co*-PEGMEMA polymers. Moreover, the fraction of H-bonded C=O increases as the concentration

of HEMA increases within the precursor formulation. This is clearly seen in the increased intensity of the vibration at 1703 cm^{-1} which corresponds to the *ν*C=O of hydrogen bonded carbonyl groups. Similarly, also the intensity of the part of overlapping O-H stretching vibrations at around 3320 cm^{-1} increases suggesting an increasing number of hydroxyl groups associated via H-bonding. Note that the latter are considered to be mainly responsible for the suppression of chain mobility promoting chain friction below the T_g of PHEMA and resulting in a rigid amorphous polymer[36] (**Figure 3b**, magnification of the -OH and -C=O stretching region; crosslinked polymers of either 100% PHEMA or PEGMEMA are used as reference).

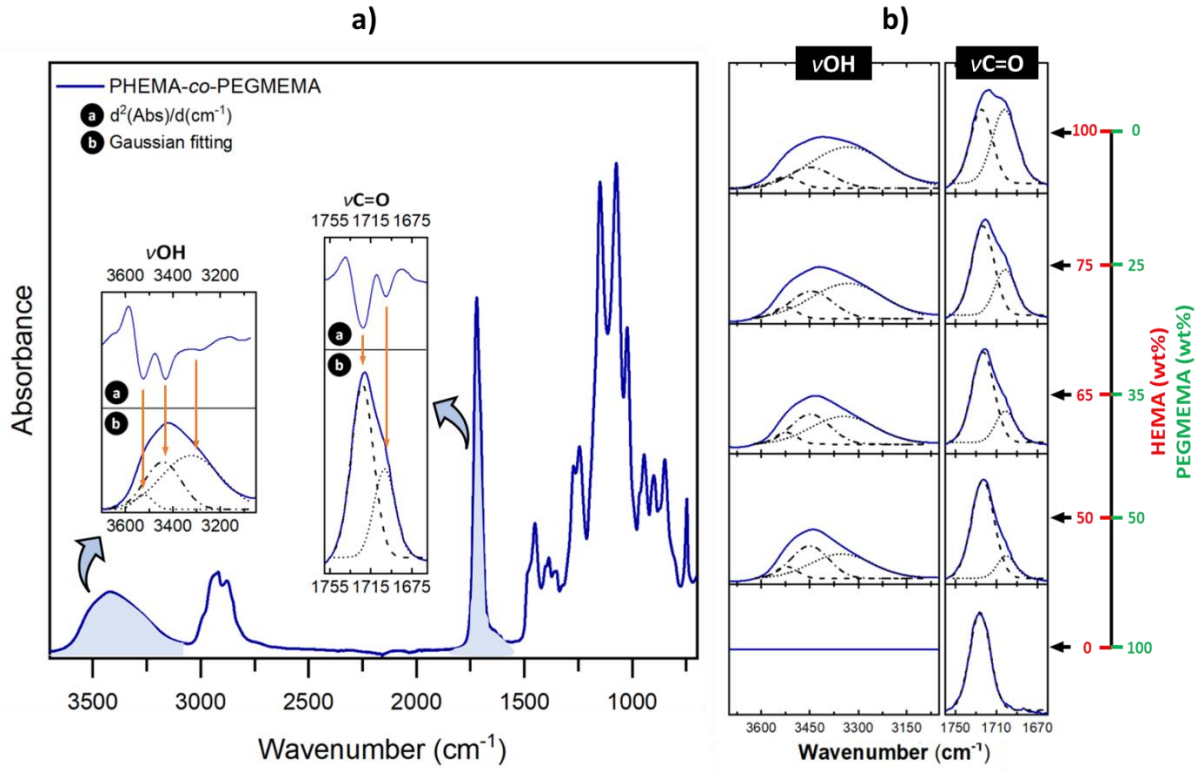

Figure 3. a) IR spectrum of a PHEMA-*co*-PEGMEMA photocured polymer with two insets displaying the second derivate spectra and the spectral components resulting from the Gaussian fitting of both the C=O an OH stretching regions; b) influence of the formulation compounding on the spectral components resulting from the Gaussian fitting of the different PHEMA-*co*-PEGMEMA polymer being investigated (crosslinked polymers prepared from precursor formulations containing 100% of either HEMA or PEGMEMA are used as reference).

These findings are in good agreement with the trend observed in the DMTA curves, since the higher density of H-bonds with increasing concentration of HEMA in the PHEMA-*co*-PEGMEMA polymers is reflected by the higher T_g. On the contrary, the T_g is lowered by adding

PEGMEMA, which serves as flexible spacer softening the network and reducing the density of available OH groups of PHEMA chains.

The significant drop of the thermomechanical properties, along with the temperature dependent reversibility of the formation of the H-bonding network and the presence of a covalently crosslinked phase that prevents chain slippage above the T_g make these PHEMA-*co*-PEGMEMA polymers promising thermoresponsive SMP candidates for DLP 4D – Printing. In order to validate this expectation, the shape memory response of all PHEMA-*co*-PEGMEMA polymers investigated in this study was evaluated by means of DMA analyses. The measurements were carried out in tensile configuration, setting a specifically designed thermo-mechanical cycle. Both the strain fixity (R_f) and the strain recovery (R_r), defined respectively as the capability of the material to hold the programmed shape and recover the permanent shape,[14,15] were evaluated quantitatively.

The plot given in **Figure 4a** shows the stress/strain evolution during the shape memory cycle of a sample from PHEMA-*co*-PEGMEMA 75:25. The thermo-mechanical cycle imposed on the sample can be described as follows. After heating the sample from room temperature to T_g+50°C = 113 °C and keeping it at this deforming temperature, T_D, for 5 min without any load, the sample is deformed under a stress of 0.02 MPa for 10 min (A → B). Subsequently, the sample is cooled down under fixed strain conditions at a cooling rate of -40 °C/min to a temperature of T_g-50°C = 13 ° (fixing temperature, T_F) in order to fix the temporary shape (B → C). Then, the load is removed (C → D). The programming temperatures T_D and T_F were set for every sample at T_g±50°C, respectively, to maximize the elasticity ratio between the glassy and rubbery state moduli, according to the DMTA curves (Figure 2a). Finally, the sample, fixed in its temporary deformed configuration, is reheated at 40 °C/min up to T_g+50°C = 113 °C under quasi stress-free conditions (0.2 kPa) to promote the recovery of the original/permanent shape (D → A).

The strain fixity parameter measured after unloading is nearly 99% (see **Table 2**, entry 3). The analysis of both the strain recovery and recovery rate during the recovering step (D → A) is reported in **Figure 4b**. The curves confirm that the polymer starts to return to its original shape when heated above its T_g, reaching a R_r ratio of about 99%. Moreover, both R_f and R_r ratios remain stable after three thermo-mechanical cycles, meaning that the material can hold the deformed configuration and recover its permanent shape with high repeatability. Similar results were observed for the samples from PHEMA-*co*-PEGMEMA 65:35 and PHEMA-*co*-PEGMEMA 50:50 (**Table 2**, entries 1 and 2).

Table 2. Results of the shape memory characterization of the samples from PHEMA-*co*-PEGMEMA X:Y (X and Y refer to weight concentration of the two photopolymerizable species in the precursor formulation); the given R_f and R_r ratios are obtained after three thermo-mechanical cycles.

Sample code	T_g [°C]	Shape memory parameters	
		R_f [%]	R_r [%]
PHEMA-*co*-PEGMEMA 50:50	12	98.6	98.7
PHEMA-*co*-PEGMEMA 65:35	27	98.6	99.0
PHEMA-*co*-PEGMEMA 75:25	63	98.8	98.8

The shape memory behavior was also confirmed qualitatively, since different 3D-printed structures revealed their ability to recover their original shape from a programmed configuration upon a thermal trigger (**Figure S3**).

The mechanism behind the thermally triggered shape memory behavior of the PHEMA-*co*-PEGMEMA polymers is proposed in **Figure 4c**, analyzing the shape memory cycle of a DLP 3D-printed structure of PHEMA-*co*-PEGMEMA 75:25 at a molecular level. The printed part is highly rigid at room temperature (RT), since the polymer is in its glassy state (T_g=63°C), and can retain its shape without deforming if loaded with a weight of 50 g. But when the temperature is increased above the T_g, the intermolecular hydrogen bonds dissociate due to a fast exchange mechanism and the mechanical properties of the polymer will depend solely on the presence of permanent covalent crosslinking points, which prevent the material from complete chain slippage.[14,15] Hence, if the load is applied above the T_g, the softened structure can be easily

deformed because the polymeric chains are sufficiently mobile to rearrange in a configuration of lower entropy. Then, the deformed configuration is fixed because the mobility of the chains is frozen out by cooling below the T_g. The temporary shape is then stabilized by the dynamic re-association of the inter- and intramolecular H-bonds, which act as additional crosslinking points of a newly formed physical network.[22] This is consistent with the high strain fixity ratios measured by means of DMA. Finally, the printed structure recovers its original shape via an entropy driven process which is determined by the permanently crosslinked network. Reheating under stress-free conditions to above the T_g, causes the H-bonding network to dissociate again allowing the molecular chains to move back into their thermodynamically preferred highest entropy state whereby the permanent shape is recovered.[14,15] After cooling to room temperature also the mechanical properties of the object are regained due to H-bond re-association.

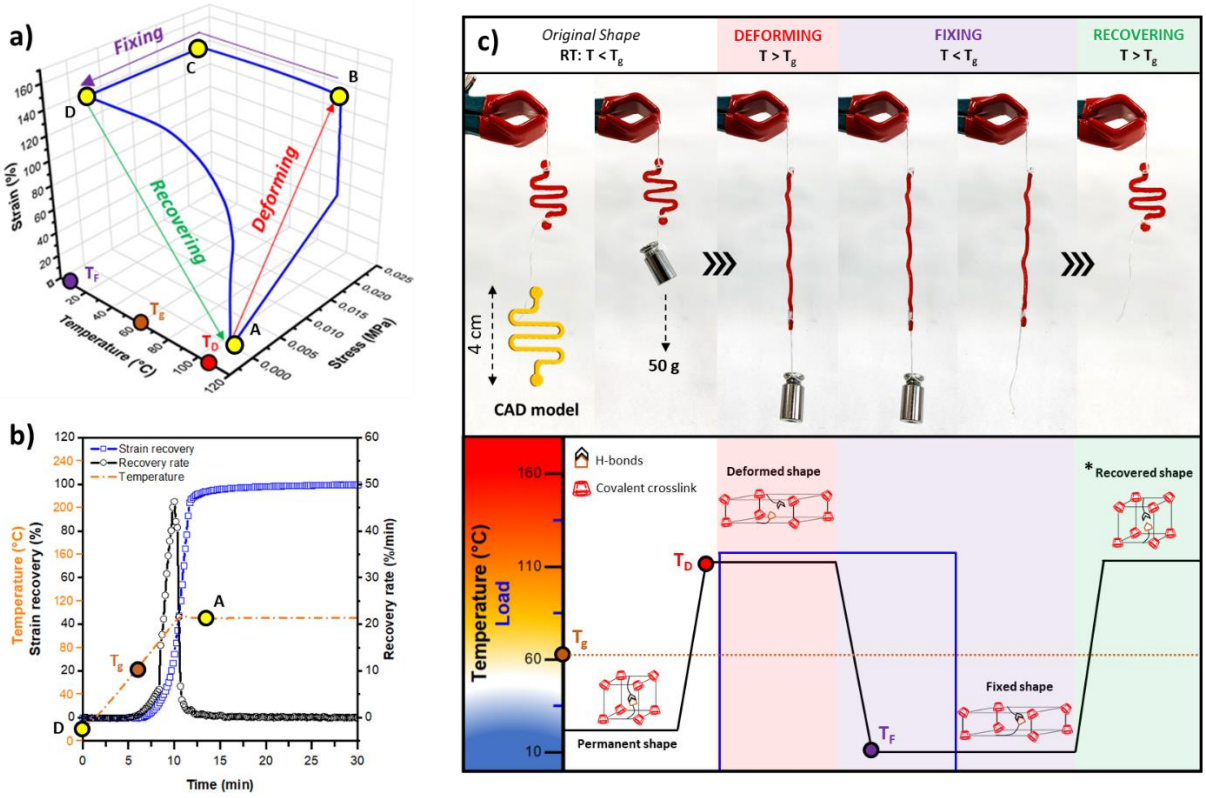

Figure 4. a) Shape memory cycle for a sample from PHEMA-*co*-PEGMEMA 75:25. A-B: heating at T_D =T_g+50°C and load application (0.02 MPa); B-C: cooling below the glass transition at T_F =T_g-50°C under fixed strain condition; C-D unloading; D-A shape recovery under quasi stress-free recovery conditions (0.2 kPa). b) evaluation of the strain recovery and

recovery rate during the recovery step (D-A). c) shape memory response of a DLP 3D – printed structure from PHEMA-*co*-PEGMEMA 75:25 and proposed molecular mechanism behind the shape memory behavior. (*) the thermodynamically stable permanent shape is recovered re-heating above the T_g, while the original mechanical properties are regained after cooling to RT, due to H-bonds re-association.

To demonstrate the potential use of such SMPs to develop 3D – printed smart devices, we fabricated a prototype of a thermoresponsive structure capable of diverting an airflow depending on its temperature.

The device (**Figure 5a** and **Figure S4**) consists of a SMP element (component 1) assembled in a double chamber box (component 2) having a single inlet duct and two separate outlets (O1 and O2, see the vertical section view given in Figure 5a). Adaptors (components 3) and PVC tubes (component 4) are used to connect the outputs of the box to two semi-open chambers (component 5) containing two pinwheels (component 6). All the components, except for the PVC connecting tubes, were DLP 3D – printed: the thermoresponsive component (1) was fabricated from PHEMA-*co*-PEGMEMA 75:25, while the other structural components (2, 3, 5 and 6) were printed from PEGDA-based formulations (see **Table S1**).

The device function can be described as follows. Before being assembled into the first chamber of the box (C1), the SMP component is programmed in a temporary vertical configuration (**Figure 5b**). The cantilever is deformed above T_g and the temporary shape (TS) is fixed by rapid cooling below T_g. Subsequently, air is blown into the device (air speed=4.5 m/s) at two different temperatures (T_1=15°C and T_2=85°C). When the inlet air temperature is lower than the T_g of the SMP component (T_1), the cantilever retains its temporary vertical configuration, locking the first outlet of the box (O1). Therefore, while the air can freely flow through O2 to make the second pinwheel spin, the airstream through O1 is blocked and the first pinwheel stands still. The pressure buildup in the diverter chamber is released from the hole located on the upper wall (**Figure 5c – left** and **Movie S1 – case A**). Whereas, if the temperature of the airstream is increased to above the T_g of the SMP diverter (T_2=85°C), the cantilever starts to

lower against the air-flow and recovers its original horizontal permanent shape (PS). Consequently, the first outlet of the box (O1) is unlocked and both the pinwheels spin (**Figure 5c – right** and **Movie S1 – case B**).

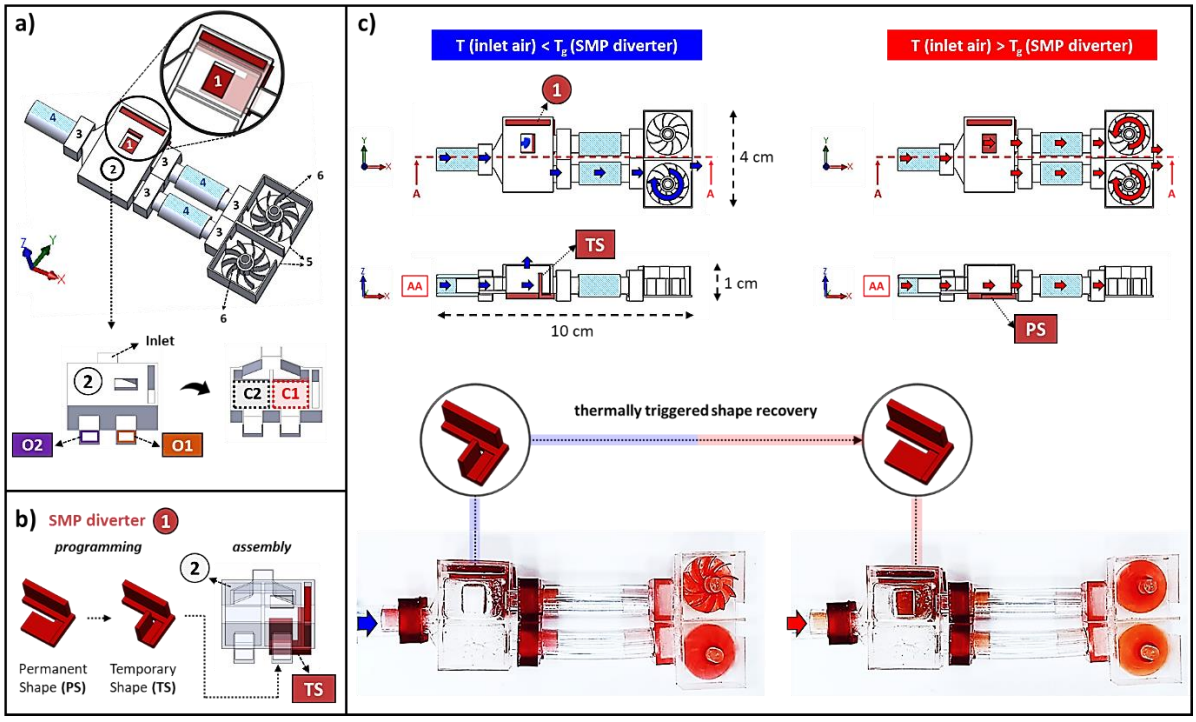

Figure 5. a) CAD model of the prototype and detail view of components 1 (top) and 2 (bottom); b) programming of the vertical configuration of the SMP diverter and assembly of the temporary shape into the box; c) functioning of the device depending on the inlet air temperature.

Another advantage of the formulations described here consists in the opportunity to design the T_g of such SMPs by simply varying the concentration of the photopolymerizable methacrylates. This property can ultimately enable the use of the same photocurable system for the fabrication of 3D – printed structures showing a sequential shape memory response, an example of which is given in **Figure 6**.

As a proof of concept, a flower-shaped structure was 3D – printed using two photocurable formulations, each one having different concentrations of HEMA and PEGMEMA and different dyes, for the fabrication of the stem and the petals. The multi-material structure is obtained by simply changing the resin vat during the printing process. Hence, after being fixed into a temporary deformed shape, the flower shows a sequential recovery upon heating. The

stem regains its permanent shape first because of its lower T_g, while the shape recovery of the flower is completed when the petals open up at higher temperatures.

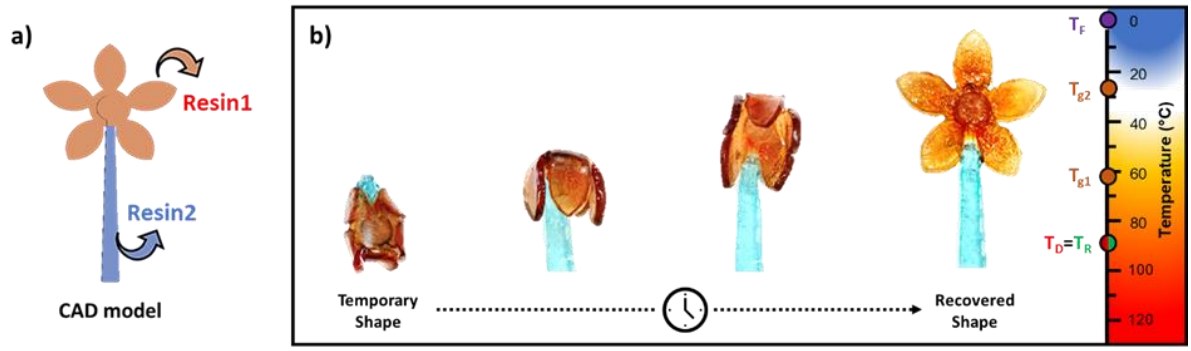

Figure 6. a) CAD model of the flower-shaped multi-material structure; b) sequential shape memory response of the printed flower. The petals are made of PHEMA-*co*-PEGMEMA 75:25 (Resin 1, T_{g1}=63°C), while the stem consist of PHEMA-*co*-PEGMEMA 65:35 (Resin 2, T_{g2}=27°C). Methyl red and brilliant green were used as dyes (0.025 phr), respectively. The programming was carried out by deforming the flower at T_D=90°C and fixing the temporary shape at T_F=3°C. The sequential shape memory response (stem first, pedals second) was observed by reheating to T_R= T_D=90°C which led to the mechanically stable shape of the flower after cooling to room temperature.

3. Conclusion

In conclusion, we proved the thermally triggered shape memory behavior of DLP 3D-printable PHEMA-*co*-PEGMEMA polymers. The shape memory response of the printed structures reveals that such materials can memorize their shape, since they are able to recover their original configuration from a mechanical deformation (strain recovery near 99%). The presence of groups which reversibly associate into an H-bonding network in dependence of the temperature allows to stabilize the programmed thermodynamically unfavorable shapes. This property is confirmed by the high values of strain fixity. Moreover, we described the influence of the H-bonding interactions on the thermo-mechanical properties and we have shown that the T_g of the PHEMA-*co*-PEGMEMA polymer can be easily tailored by varying the concentration of the photopolymerizable ingredients in the precursor formulation. This gives the opportunity to prepare DLP 3D – printable materials having shape memory behavior at different temperature by simply adjusting the formulation compounding.

Finally, a thermoresponsive airflow diverter was successfully fabricated, envisaging the potential use of such PHEMA-*co*-PEGMEMA shape memory polymers for the development of smart 3D – printed devices.

Experimental Section

Materials: 2-Hydroxyethyl methacrylate (HEMA, ≥99%, contains ≤50 ppm monomethyl ether hydroquinone as inhibitor), poly(ethylene glycol) methyl ether methacrylate (PEGMEMA, Mn = 500 g/mol, contains 200 ppm BHT as inhibitor, 100 ppm MEHQ as inhibitor), 2-(4-Dimethylaminophenylazo)benzoic acid (Acid Red 2 or Methyl red) and brilliant green (hydrogen sulfate) were purchased from Sigma Aldrich and used as received. The phosphaneoxide derivative BAPO-γ-CyD was prepared according to a synthetic protocol reported in a previous work[32] and used as multiple photoinitiator and photocrosslinking agent at once.

Photorheology: The photopolymerization kinetic of the formulations was investigated by means of real-time photorheology using an Anton PAAR Modular Compact Rheometer (Physica MCR 302, Graz, Austria) in parallel-plate mode (25 mm diameter, gap between the two plates set to 0.2 mm). The measurements were carried out at room temperature (RT, 25°C) keeping the sample under a constant shear frequency (10 Hz), while a UV-light source (Hamamatsu LC8 lamp equipped with a 8 mm optical fiber, 30 mW/cm^2) irradiates the quartz plate from the bottom. The light was switched on after 60 s to let the system stabilize before the onset of polymerization. The evolution of both the storage and loss moduli (G' and G'', respectively) during the irradiation was recorded, as well as the onset of photopolymerization (i.e. the delay time required to induce crosslinking) and the curing rate (measured as the slope of the curve in the first 20 s of irradiation).

DLP 3D – printing: The photocurable formulations were 3D printed using an ASIGA UV-MAX X27 DLP printer (XY pixel resolution of 27 μm; diode source emitting at 385 nm

and building volume of 119 mm x 67 mm x 75 mm). Different 3D models were designed using Solidworks 2019 CAD software, converted in STL file formats and 3D – printed. The vat surface was wetted with silicon oil to avoid the adhesion of the photocured methacrylates while printing. The layer thickness and the light intensity were fixed at 25 μm and 32 mW/cm^2, while the exposure time was specifically selected for each specific formulation, based on the photorheology measurements. Lastly, the printed objects were post-cured for 3 min under UV-light (12 mW/cm^2, medium-pressure mercury lamp provided by Robot Factory).

Gel Content: The gel content was measured to evaluate the covalently crosslinked fraction of the printed polymers (insoluble fraction). The samples were held in a net having a fine mesh, weighed and immersed in water for 24 h to dissolve the un-crosslinked polymer (soluble fraction). Then, the samples were dried in a vacuum oven (80 °C, 100 mbar) until no mass variation is detected. The gel content (GC%) was determined as follows:

$$GC\ (\%) = \frac{m_{dried}}{m_0}\ x\ 100$$

where m_{dried} is the residual mass after the extraction, while m_0 is the initial mass of the sample. The results were averaged over three measurements.

Dynamic Mechanical Thermal Analysis measurements: Thin rectangular samples were prepared by UV – curing and used for the thermo-mechanical characterizations. The precursor formulations were casted into silicon molds and irradiated for 5 min at RT with UV light (Hamamatsu LC8 lamp equipped with an 8 mm optical fiber, 130 mW/cm^2). Dynamic mechanical thermal analyses (DMTAs) were carried out using a Tritec 2000 DMA (Triton Technology Ltd, London UK), setting a temperature ramp of 3°C/min and applying a force to the sample under a frequency of 1 Hz with a displacement of 20 μm. The evolution of both the conservative and loss modului (E' and E'', respectively) and the damping factor (tanδ) during the temperature ramp was recorded. The glass transition temperature (T_g) was taken as the temperature corresponding to the tanδ peak, as recommended by traditional conventions.

IR measurements: Attenuated total reflectance Fourier transform infrared spectroscopy (ATR-FT-IR) was used to evaluate the H-bonding interactions in the PHEMA-*co*-PEGMEMA polymers. The experiments were conducted on dried thin photocured films (5 min irradiation at RT, using a Dymax ECE 5000-UV lamp), using a Thermo Scientific Nicolet iS50 FTIR Spectrometer (Milano, Italy) equipped with a diamond crystal ATR accessory. For each sample, 64 spectra were collected in the range of 4000–600 cm^{-1}, with a resolution of 4 cm^{-1}. The results were acquired with Omnic software and analyzed with Origin 2018 software. Second derivative spectra were calculated in the regions of the OH and C=O stretching vibrations (3700-3300 and 1700-1730 cm^{-1}, respectively) and the resulting plots were smoothed with the Savitzky-Golay method. Then, the peak deconvolution of the spectral bands in the aforementioned regions was evaluated *via* Gaussian fitting in order to identify the spectral contributes.

Shape memory behavior: The shape memory measurements were carried out on flat rectangular specimens (same as those used for the previous DMTAs) using a DMA Q800 (Thermal Analysis Inc.) in tensile configuration. Specifically designed thermo-mechanical histories were applied on the samples and the shape memory response was evaluated following the stress/strain evolution. The shape memory cycles involve a programming step followed by a recovery step. In the programming step the specimen is deformed above the glass transition temperature (T_g + 50°C) under a stress of 0.02 MPa, and the temporary shape is fixed by cooling the deformed configuration below the glass transition temperature (T_g - 50°C; temperature ramp of -40°C/min) under fixed strain conditions. Finally, in the recovery step the sample is heated again at T_g + 50°C (temperature ramp of 10°C/min) under quasi stress-free condition (applied stress of 0.2 kPa) and the shape memory response was evaluated by monitoring the strain evolution as a function of temperature. The ability of the samples to hold the strained configuration and to recover their original shape, defined as strain fixity (R_f) and strain recovery (R_r) respectively, are calculated as follows:

$$R_f = \frac{\varepsilon_u(N)}{\varepsilon_l(N)}$$

where ε_l (N) is the strain achieved after cooling at low temperature and ε_u (N) is the strain after unloading for the Nth cycle.

$$R_R = \frac{\varepsilon_l(N) - \varepsilon_r(N)}{\varepsilon_l(N) - \varepsilon_r(N-1)}$$

where ε_r (N) and ε_r (N-1) are the residual strains after the recovery step for two consecutive thermo-mechanical cycles.

Moreover, also the recovery rate was calculated as the first derivative of the strain recovery curve,

Supporting Information
Supporting Information is available from the Wiley Online Library or from the author.

Acknowledgements

This work was performed with the financial support of Compagnia di San Paolo.

Received: ((will be filled in by the editorial staff))
Revised: ((will be filled in by the editorial staff))
Published online: ((will be filled in by the editorial staff))

References

[1] A. Lendlein, R. Langer, *Science* **2002**, *296*, 1673.

[2] S. Neuss, I. Blomenkamp, R. Stainforth, D. Boltersdorf, M. Jansen, N. Butz, A. Perez-Bouza, R. Knüchel, *Biomaterials* **2009**, *30*, 1697.

[3] A. Metcalfe, A. C. Desfaits, I. Salazkin, L. Yahia, W. M. Sokolowski, J. Raymond, *Biomaterials* **2003**, *24*, 491.

[4] J. L. Reed, Jr., C. D. Hemmelgarn, B. M. Pelley, E. Havens, In *Smart Structures and Materials 2005: Industrial and Commercial Applications of Smart Structures*

Technologies (Ed.: White, E. V.), SPIE, **2005**, p. 132.

[5] X. Lan, Y. Liu, H. Lv, X. Wang, J. Leng, S. Du, *Smart Mater. Struct.* **2009**, *18*, 024002.

[6] A. Browne, 309,104 NL Johnson - US Patent 7, undefined 2007, *Shape memory polymer seat assemblies*, **2007**.

[7] K. Gall, P. Kreiner, D. Turner, M. Hulse, *J. Microelectromechanical Syst.* **2004**, *13*, 472.

[8] H. Takehara, C. Jiang, K. Uto, M. Ebara, T. Aoyagi, T. Ichiki, *Appl. Phys. Express* **2013**, *6*, 037201.

[9] T. Sekitani, U. Zschieschang, H. Klauk, T. Someya, *Nat. Mater.* **2010**, *9*, 1015.

[10] Z. Yu, Q. Zhang, L. Li, Q. Chen, X. Niu, J. Liu, Q. Pei, *Adv. Mater.* **2011**, *23*, 664.

[11] D. Ratna, J. Karger-Kocsis, *J. Mater. Sci.* **2008**, *43*, 254.

[12] J. Hu, Y. Zhu, H. Huang, J. Lu, *Recent advances in shape-memory polymers: Structure, mechanism, functionality, modeling and applications*, Vol. 37, Pergamon, **2012**, pp. 1720–1763.

[13] B. Gyarmati, B. Á. Szilágyi, A. Szilágyi, *Reversible interactions in self-healing and shape memory hydrogels*, Vol. 93, Elsevier Ltd, **2017**, pp. 642–669.

[14] C. L. Lewis, E. M. Dell, *A review of shape memory polymers bearing reversible binding groups*, Vol. 54, John Wiley and Sons Inc., **2016**, pp. 1340–1364.

[15] T. Xie, *Recent advances in polymer shape memory*, Vol. 52, Elsevier Ltd, **2011**, pp. 4985–5000.

[16] M. Anthamatten, S. Roddecha, J. Li, *Macromolecules* **2013**, *46*, 4230.

[17] B. Heuwers, A. Beckel, A. Krieger, F. Katzenberg, J. C. Tiller, *Macromol. Chem. Phys.* **2013**, *214*, 912.

[18] G. Rabani, H. Luftmann, A. Kraft, *Polymer (Guildf).* **2006**, *47*, 4251.

[19] S. Pandini, S. Passera, M. Messori, K. Paderni, M. Toselli, A. Gianoncelli, E.

Bontempi, T. Ricc, *Polymer (Guildf).* **2012**, *53*, 1915.

[20] M. Messori, M. Degli Esposti, K. Paderni, S. Pandini, S. Passera, T. Riccò, M. Toselli, *J. Mater. Sci.* **2013**, *48*, 424.

[21] S. Pandini, F. Baldi, K. Paderni, M. Messori, M. Toselli, F. Pilati, A. Gianoncelli, M. Brisotto, E. Bontempi, T. Riccò, *Polymer (Guildf).* **2013**, *54*, 4253.

[22] J. Li, J. A. Viveros, M. H. Wrue, M. Anthamatten, *Adv. Mater.* **2007**, *19*, 2851.

[23] J. Li, C. L. Lewis, D. L. Chen, M. Anthamatten, *Macromolecules* **2011**, *44*, 5336.

[24] G. Liu, C. Guan, H. Xia, F. Guo, X. Ding, Y. Peng, *Macromol. Rapid Commun.* **2006**, *27*, 1100.

[25] T. Ware, K. Hearon, A. Lonnecker, K. L. Wooley, D. J. Maitland, W. Voit, *Macromolecules* **2012**, *45*, 1062.

[26] X. Kuang, D. J. Roach, J. Wu, C. M. Hamel, Z. Ding, T. Wang, M. L. Dunn, H. J. Qi, *Advances in 4D Printing: Materials and Applications*, Vol. 29, Wiley-VCH Verlag, **2019**.

[27] Y. Xia, Y. He, F. Zhang, Y. Liu, J. Leng, *Adv. Mater.* **2020**, 2000713.

[28] H. Chu, W. Yang, L. Sun, S. Cai, R. Yang, W. Liang, H. Yu, L. Liu, *4D printing: A review on recent progresses*, Vol. 11, MDPI AG, **2020**, p. 796.

[29] E. Sachyani Keneth, A. Kamyshny, M. Totaro, L. Beccai, S. Magdassi, *Adv. Mater.* **2020**, 2003387.

[30] Q. Ge, A. H. Sakhaei, H. Lee, C. K. Dunn, N. X. Fang, M. L. Dunn, *Sci. Rep.* **2016**, *6*.

[31] M. Zarek, M. Layani, I. Cooperstein, E. Sachyani, D. Cohn, S. Magdassi, *Adv. Mater.* **2016**, *28*, 4449.

[32] A. Cosola, R. Conti, V. K. Rana, M. Sangermano, A. Chiappone, J. Levalois-Grützmacher, H. Grützmacher, *Chem. Commun.* **2020**, *56*, 4828.

[33] C. L. Lewis, K. Stewart, M. Anthamatten, *Macromolecules* **2014**, *47*, 729.

[34] S. W. Kuo, H. T. Tsai, *Macromolecules* **2009**, *42*, 4701.

[35] J. M. Chalmers, P. R. Griffiths, *Handbook of Vibrational Spectroscopy*, Wiley, Chichester, UK, **2002**.

[36] S. Morita, *Front. Chem.* **2014**, *2*, 10.

[37] S. Morita, K. Kitagawa, Y. Ozaki, *Vib. Spectrosc.* **2009**, *51*, 28.

[38] S. Morita, M. Tanaka, Y. Ozaki, *Langmuir* **2007**, *23*, 3750.

Table of content entry:

The fabrication of materials capable of transforming with time under the application of an external stimulus is a new challenge of additive manufacturing.
Here, we present a photopolymerizable system based on monofunctional methacrylates to prepare shape memory polymers (SMPs) stabilized by thermoreversible hydrogen bonding interactions, which can be integrated to develop smart devices *via* DLP 3D – printing.

Andrea Cosola, Marco Sangermano, Davide Terenziani, Riccardo Conti, Massimo Messori, Hansjörg Grützmacher and Annalisa Chiappone*

DLP 3D – printing of shape memory polymers stabilized by thermoreversible hydrogen bonding interactions

ToC figure:

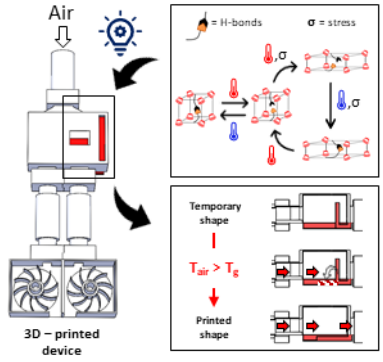

Supporting Information

DLP 3D – printing of shape memory polymers stabilized by thermoreversible hydrogen bonding interactions

Andrea Cosola, Marco Sangermano, Davide Terenziani, Riccardo Conti, Massimo Messori, Hansjörg Grützmacher and Annalisa Chiappone*

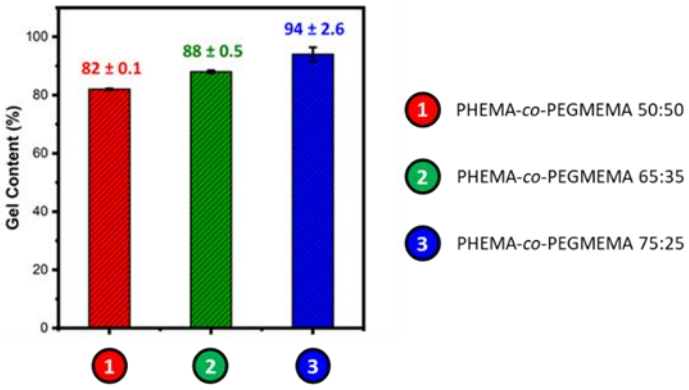

Figure S1. Gel content values for all the PHEMA-*co*-PEGMEMA polymers being investigated in this study.

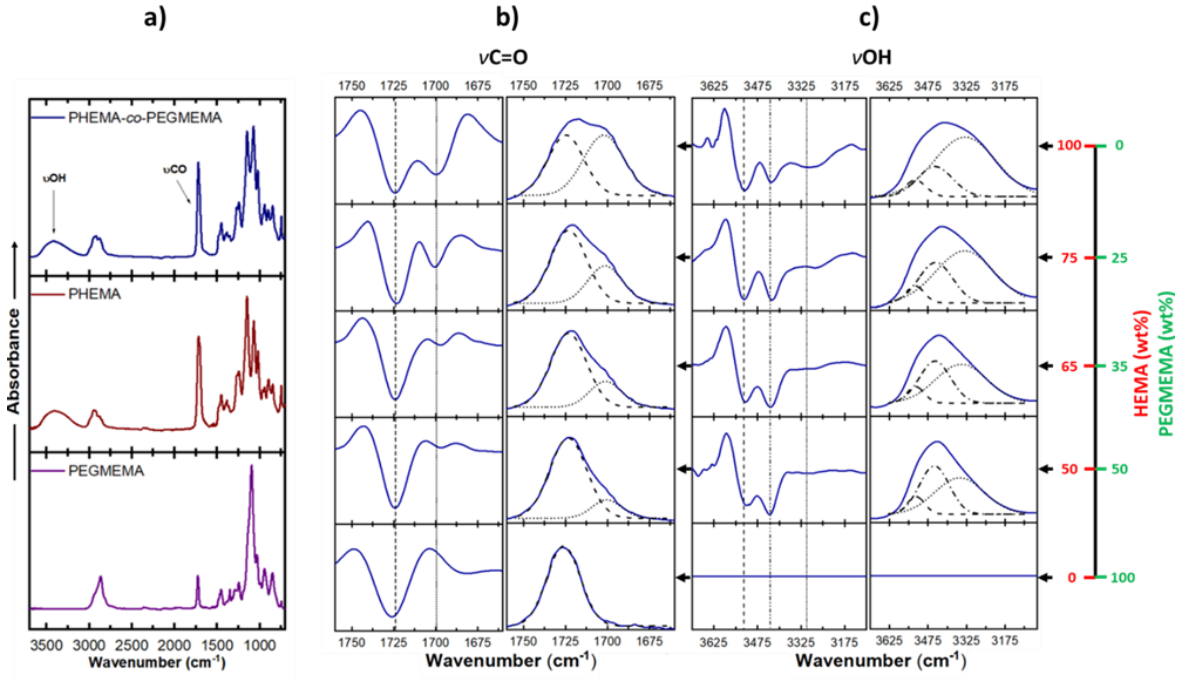

Figure S2. a) comparison between the IR spectra of photo-crosslinked PHEMA-*co*-PEGMEMA, PHEMA (100%) and PEGMEMA (100%) polymers; influence of the formulation compounding on the second derivate spectra and spectral components resulting from the gaussian fitting of both the C=O an OH stretching regions (b and c, respectively).

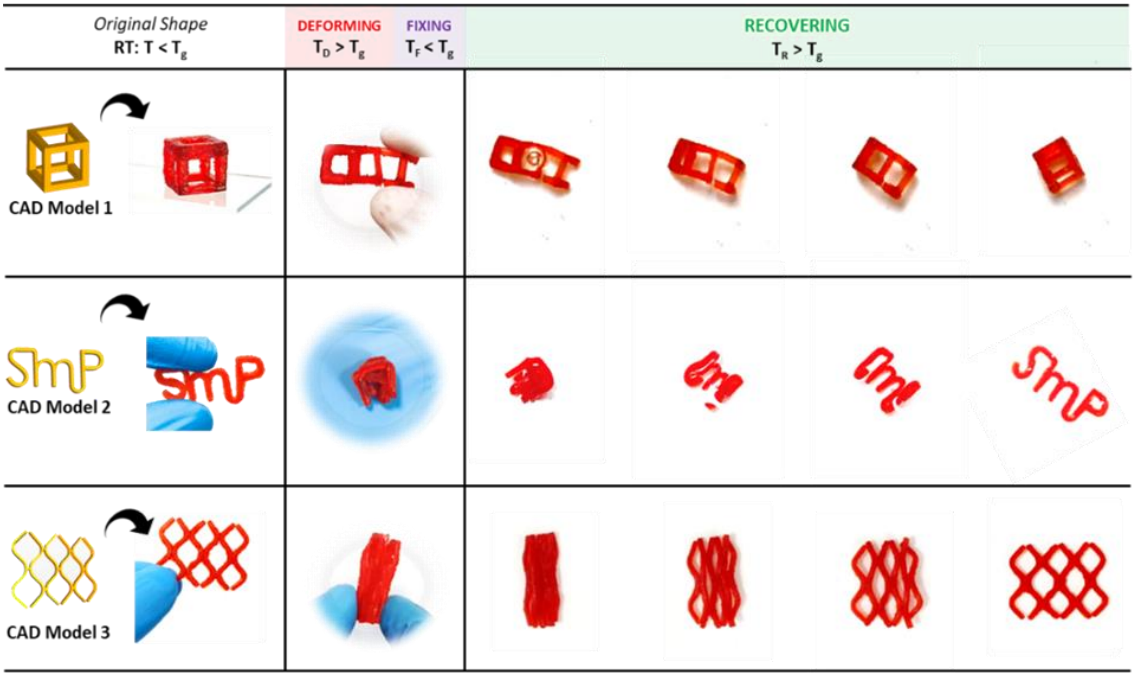

Figure S3. Shape memory cycles of different DLP – printed structures from PHEMA-*co*-PEGMEMA 65:35. Temporary shape programmed by deforming the structures above the T_g (T_D =70°C) and fixing the strained configuration by rapid cooling below the T_g (T_F =3°C). The shape recovery is carried out in water heated to above the T_g (T_R=T_D=70°C).

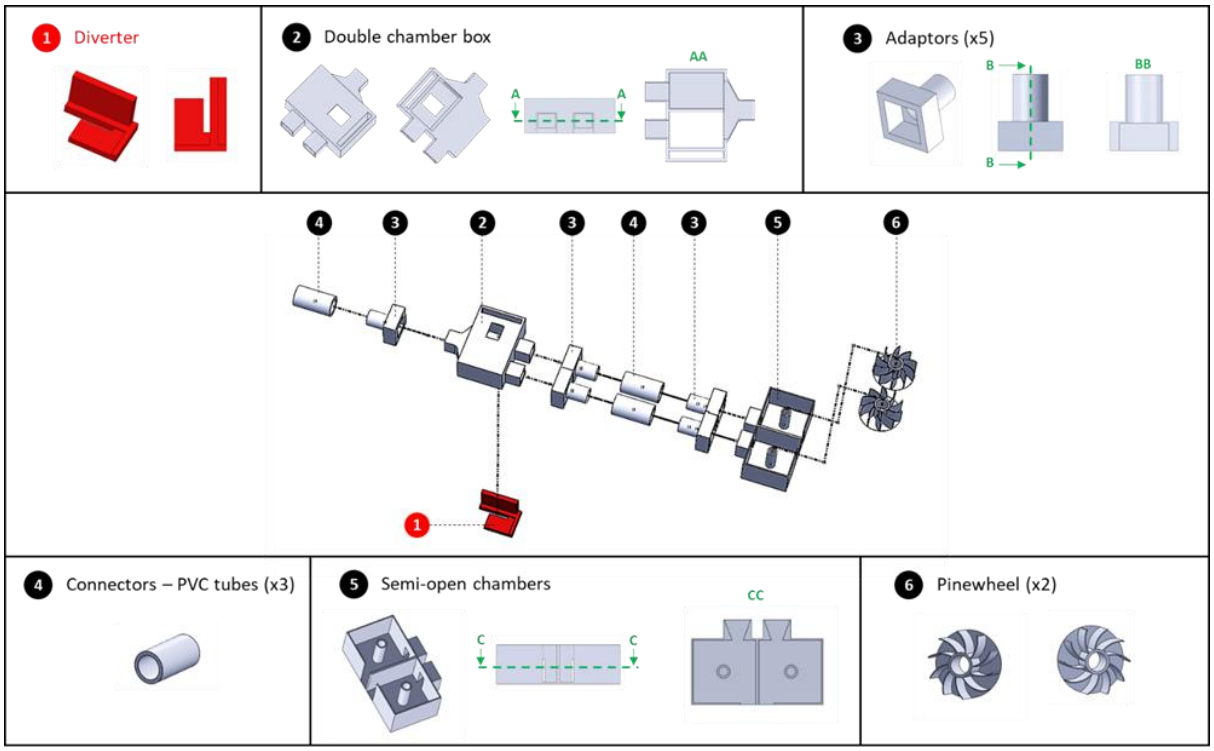

Figure S4. CAD models of the device components with assembly instructions.

Table S1. Photocurable PEGDA-based formulations used for the fabrication of components 2, 3, 5 and 6.

Components	PEGDA (Mn=250) [wt%]	BAPO-Ph [wt%]	Methyl red [phr]
2	99.5	0.5	-
3			0.02
5			-
6			0.02